Synthesis, Crystal Structures and Spectroscopic Properties of RbBaTaS$_4$ and K$_2$BaTa$_2$S$_{11}$

Yuandong Wu and Wolfgang Bensch

Institut für Anorganische Chemie, Universität Kiel, Max-Eyth-Straße 2, 24118 Kiel, Germany

Reprint requests to Prof. W. Bensch. Fax: +49-431-880-1520. E-mail: wbensch@ac.uni-kiel.de

Single crystals of RbBaTaS$_4$ (**1**) and K$_2$BaTa$_2$S$_{11}$ (**2**) were obtained from the reactions of Ta, with *in situ* formed fluxes of A_2S$_3$ (A = K, Rb), BaS, and S at 500 °C. Compound **1** crystallizes in the orthorhombic space group *Pnma* with a = 9.3286(5), b = 7.0391(4), c = 12.4365(7) Å, V = 816.6(1) Å^3, Z = 4. Compound **2** crystallizes in the monoclinic space group $P2_1/c$ with a = 14.5280(10), b = 12.6347(7), c = 17.5148(12) Å, β = 94.744(8)°, V = 3203.9(4) Å^3, Z = 4. The structure of RbBaTaS$_4$ (**1**) consists of isolated tetrahedral [TaS$_4$]$^{3-}$ anions and Rb$^+$ and Ba^{2+} cations. The Ba^{2+} cations are surrounded by nine sulfur atoms forming distorted tricapped trigonal prisms, whereas the Rb$^+$ cations are in an irregular environment of ten sulfur atoms. The structure of K$_2$BaTa$_2$S$_{11}$ (**2**) consists of two different dinuclear [Ta$_2$S$_{11}$] units which are separated by Ba^{2+} and K$^+$ cations. The Ta atoms are coordinated by S$_2^{2-}$ and S^{2-} ligands according to the mode [Ta$_2(\mu_2$-S$)(\mu_2$-η^2,η^1-S$_2)_2(\eta^2$-S$_2)_2$(S)$_2$]$^{4-}$. Each Ta atom is surrounded by seven sulfur ions forming strongly distorted pentagonal bipyramids. The two [TaS$_7$] polyhedra share a common face in the [Ta$_2$S$_{11}$] unit. The K$^+$ and Ba^{2+} cations are statistically distributed over the crystallographic sites. Compound **2** has also been characterized by UV/Vis diffuse reflectance, IR and Raman spectroscopy.

Key words: Alkali Polysulfide Flux, Barium, Tantalum Thiophosphates, Crystal Structure, Spectroscopic Properties

Introduction

In the last two decades, a large number of new compounds in the alkali metal/group 5 element/chalcogen systems were prepared and extensively investigated due to their interesting chemical and physical properties. Most compounds are characterized by [MQ_4]$^{3-}$ and [M_2Q_{11}]$^{4-}$ (M = V, Nb, Ta, Q = S, Se) building blocks as the basic structural motifs [1 – 24]. Among the A_3MQ_4 (A = Na, K, Rb, Cs; M = V, Nb, Ta; Q = S, Se) compounds Na$_3$VS$_4$ [1] crystallizes in the tetragonal space group $P\bar{4}2_1c$ (no. 114) whereas Na$_3$NbS$_4$ [5] and Na$_3$TaS$_4$ [5, 8] belong to the orthorhombic space group Fdd2 (no. 43). All K, Rb, Cs compounds crystallize in the orthorhombic space group *Pnma* (no. 62) and are of the K$_3$VS$_4$ structure type. The tetrahedral [MQ_4]$^{3-}$ anions have crystallographically imposed m symmetry with the metal atom located on the special position $4c$. The two crystallographically unique alkali metal cations ($4c$ and $8d$) in the K and Rb compounds are coordinated by seven Q atoms of four and six [MQ_4]$^{3-}$ ions, respectively. In the Cs compounds,

one type of Cs$^+$ cations located on the special position $4c$ is coordinated by five Q atoms and a second type on the general position $8d$ is surrounded by seven Q atoms in irregular polyhedra. The [M_2Q_{11}] units are either isolated monomeric anions in $A_4M_2Q_{11}$ (A = K, Rb, Cs, Tl; M = Nb, Ta; Q = S, Se) [12, 17 – 20, 25, 26], or connected *via* terminal Q_n^{2-} ligands like in A_6M_4S$_{22}$ (A = K, Rb, Cs; M = Nb, Ta) [15, 16, 21, 27], A_6M_4S$_{25}$ (A = K, Rb; M = Nb, Ta) [13, 22], and $A_{12}M_6$Se$_{35}$ (A = K, Rb; M = Nb, Ta) [23, 24]. These polychalcogenides were obtained by reacting Nb or Ta powders in molten alkali polychalcogenide fluxes at intermediate temperatures ($<$ 873 K). The formation of the different structural motifs depends on the reaction temperature as well as on the composition of the fluxes [28 – 30].

As a part of our ongoing synthetic work using the reactive flux method, we have recently reported the compounds KBaNbS$_4$ [31], K$_2$BaNb$_2$S$_{11}$ [32], and Rb$_2$BaNb$_2$Se$_{11}$ [33]. In the structure of KBaNbS$_4$, the [NbS$_4$]$^{3-}$ tetrahedra are stacked along the [100] direction, and a modulation leads to a slight tilting of the anions against each other. The K$^+$ and Ba^{2+}

cations follow this tilting by being slightly shifted from their position in the average structure. In the structure of K$_2$BaNb$_2$S$_{11}$, two different [Nb$_2$S$_{11}$]$^{4-}$ anions are found due to the occurrence of statistically distributed Ba^{2+}/K$^+$ cations. Both anions have a very similar topology but are surrounded by a different number of Ba^{2+} and K$^+$ cations, respectively. The structure of the polyselenide Rb$_2$BaNb$_2$Se$_{11}$ contains a one-dimensional anionic $_\infty^1$[Nb$_2$Se$_{11}$]$^{4-}$ chain separated by Rb$^+$ and Ba^{2+} cations. The chain is formed by interconnection of dinuclear [Nb$_2$Se$_{11}$] units through Se$_2$$^{2-}$ anions, formed in a face-sharing of two NbSe$_7$ pentagonal bipyramids.

In continuing experiments we tried to prepare quaternary group 1/group 2 tantalum chalcogenides using the reactive flux method. It is of special interest to find out whether compounds can be prepared which are still based on [TaS$_4$]$^{3-}$ and [Ta$_2$S$_{11}$]$^{4-}$ units like the niobium compounds mentioned above, and how the alkaline earth and/or alkali cations influence the composition and structure of the new compounds. Here we report the synthesis, structural characterization, and optical properties of the first group 1/group 2 tantalum sulfides RbBaTaS$_4$ (**1**) and K$_2$BaTa$_2$S$_{11}$ (**2**).

Experimental Section

Reagents

The following reagents were used as purchased: K (99.5 %, Strem), Rb (99.5 %, Strem), Ta (99.97 %, Fluka), S (99.99 %, Heraeus), BaS (99.99 %, Alfa).

Synthesis

K$_2$S$_3$ and Rb$_2$S$_3$ were prepared from a stoichiometric mixture of the elements in liquid ammonia under an argon atmosphere.

Preparation of RbBaTaS$_4$ (1)

RbBaTaS$_4$ (**1**) was prepared by reacting a mixture of Rb$_2$S$_3$, BaS, Ta, and S in a 1 : 1 : 1 : 4 molar ratio. The mixture was thoroughly ground in an N$_2$-filled glove box and loaded into a glass ampoule. After evacuation to $\sim 10^{-3}$ mbar the ampoule was flame-sealed and placed in a computer-controlled furnace. The mixture was heated to 500 °C at a rate of 0.5 °C min^{-1}, kept at this temperature for 6 d before the sample was cooled down to 100 °C at a rate of 2 °C h^{-1}, followed by cooling to r. t. within 10 h. The product was washed with dry N,N-dimethylformamide and acetone yielding transparent pink polyhedra of compound **1** (yield about 90 % based on Ta). The compound is stable in

dry air. EDX analyses performed on freshly cleaved faces of several crystals indicated the presence of all four elements (Rb, Ba, Ta, S), and for all crystals the atomic ratio was identical amounting to the ratio 1 : 1 : 1 : 4.

Preparation of K$_2$BaTa$_2$S$_{11}$ (2)

Powders of K$_2$S$_3$, BaS, Ta, and S in a 1 : 0.75 : 1 : 4 molar ratio were thoroughly mixed in an N$_2$-filled glove box and loaded into a glass ampoule which was evacuated (1 × 10^{-3} mbar) and flame-sealed. The tube was placed in a computer-controlled furnace and heated to 500 °C within 24 h. After 6 d the sample was cooled down to 100 °C at a rate of 2 °C h^{-1} followed by cooling to r. t. in 4 h. Excess flux was removed by washing the reaction product with N,N-dimethylformamide and acetone. The product consisted of transparent red-orange platelets K$_2$BaTa$_2$S$_{11}$ (yield ~ 60 % based on Ta) and transparent pink platelets KBaTaS$_4$ (EDX; ~ 40 %). Attempts to synthesize pure K$_2$BaTa$_2$S$_{11}$ and KBaTaS$_4$ were unsuccessful until now. Compound **2** is stable in air for several weeks. An EDX analysis indicated the presence of all four elements (K, Ba, Ta, S) in an approximate atomic ratio of 2.3 : 1 : 2.1 : 11.4.

X-Ray crystallography

Data sets of selected crystals of both compounds were collected on a Stoe Imaging Plate Diffraction System (IPDS-1) with graphite-monochromatized MoK_α radiation ($\lambda = 0.7107$ Å) at -93 °C. Size of crystal **1**: 0.12 × 0.09 × 0.07 mm^3; crystal **2**: 0.15 × 0.11 × 0.06 mm^3. The raw intensities were corrected for Lorentz, polarization and absorption. The structures were solved with Direct Methods and refined with full-matrix least-squares techniques using the SHELXTL software package [34].

RbBaTaS$_4$. The structure was solved and refined successfully in space group *Pnma*. The final cycle of refinement performed with 1069 unique reflections converged to residuals $wR2$ ($F_o^2 > 0$) = 0.0493, and the conventional R index based on reflections $F_o^2 \geq 2\ \sigma(F_o^2)$ was 0.0202. The resulting structural model of compound **1** was standardized using the program STRUCTURE TIDY [35] in PLATON [36].

K$_2$BaTa$_2$S$_{11}$. From the systematic absence conditions of the data set the space group *P2$_1$/c* was selected. Initial positions of all atoms were found by Direct Methods using SHELXS-97 [34]. The refinement assuming the ideal formula "K$_2$BaTa$_2$S$_{11}$" was performed using SHELXL-97 [34]. However, the difference Fourier map revealed considerable residual electron density located in the proximity of some of the potassium cations. In addition, some of these atoms showed non-positive principal mean square atomic displacement parameters. Therefore mixed occupancies of all K sites with Ba and all Ba sites with K were introduced. To minimize ar-

Table 1. Crystallographic data and details of the structure determinations of RbBaTaS$_4$ (**1**) and K$_2$BaTa$_2$S$_{11}$ (**2**).

Formula	RbBaTaS$_4$	K$_2$BaTa$_2$S$_{11}$
Crystal color	pink	red
Temperature, K	180	180
Crystal system	orthorhombic	monoclinic
Space group	$Pnma$ (no. 62)	$P2_1/c$ (no. 14)
a, Å	9.3286(5)	14.5280(10)
b, Å	7.0391(4)	12.6347(7)
c, Å	12.4365(7)	17.5148(12)
β, deg	90	94.744(8)
V, Å^3	816.64(8)	3204.0(4)
Z	4	8
Calcd. density, g cm^{-3}	4.33	3.83
μ, mm^{-1}	25.0	17.8
$F(000)$, e	920	3309.5
2θ range, deg	5 – 56	5 – 56
Index range hkl	$\pm12, \pm9, \pm16$	$-19 \to 17, -16 \to 15,$ ±23
Trans. min. / max.	0.0358 / 0.0832	0.116 / 0.317
Refl. collect. / indep. /	6783 / 1069 /	21960 / 7668 /
R_{int}	0.0499	0.0589
Refl. with $F_o \geq 4\sigma(F_o)$	1028	6488
No. of ref. params	41	296
$R1^a$ for $F_o \geq 4\sigma(F_o)$	0.0202	0.0408
$wR2^b$ for all reflections	0.0493	0.1091
Weighting scheme: A^b	0.0237	0.0726
GoF^c	1.108	1.024
$\Delta\rho$ (max. / min.), e Å^{-3}	1.40 / −1.65	3.14 / −4.78

^{a} $R1 = \Sigma||F_o| - |F_c||/\Sigma|F_o|$; ^{b} $wR2 = [\Sigma w(F_o{}^2 - F_c{}^2)^2/\Sigma w(F_o{}^2)^2]^{1/2}$, $w = [\sigma^2(F_o{}^2) + (AP)^2]^{-1}$, where $P = (\text{Max}(F_o{}^2, 0) + 2F_c{}^2)/3$; ^{c} GoF $= [\Sigma w(F_o{}^2 - F_c{}^2)^2/(n_{\text{obs}} - n_{\text{param}})]^{1/2}$.

tifacts which may be associated with the correlation between K and Ba atoms, refinements at this stage were performed stepwise. The site occupation factors of K and Ba atoms on each site were allowed to refine individually while the sum of K and Ba occupation factors was constrained to full occupancy on these crystallographic sites. The K and Ba atoms on each site were refined with the same coordinates and the same anisotropic displacement factors using the EXYZ and EADP option in SHELXL-97 [34]. The refinement converged to reasonable reliability factors, and the composition was refined to K$_{2.06(1)}$Ba$_{0.94(1)}$Ta$_2$S$_{11}$. In all space groups of lower symmetry the disorder remained identical. Using the ADDSYM option [37] in PLATON [36] always space group $P2_1/c$ is suggested. Long exposed images gave no hints for a superstructure.

The parameters for data collection and the details of the structural refinements for the two compounds are summarized in Table 1. Atomic coordinates and isotropic displacement parameters are given in Tables 2 (**1**) and 3 (**2**). Selected bond lengths and angles are listed in Tables 4 (**1**) and 5 (**2**).

Further details of the crystal structure investigation may be obtained from Fachinformationszentrum Karlsruhe, 76344 Eggenstein-Leopoldshafen, Germany (fax: +49-7247-

Table 2. Atomic coordinates and equivalent isotropic displacement parameters U_{eq} (Å$^2 \times 10^3$) for RbBaTaS$_4$.*

Atom	W.-site	x	y	z	U_{eq}
Ta	4c	0.27019(3)	1/4	0.42052(2)	7(1)
Ba	4c	0.01929(4)	1/4	0.82389(3)	11(1)
Rb	4c	0.36383(7)	1/4	0.08958(6)	18(1)
S(1)	8d	0.18455(14)	0.50886 (16)	0.33613(9)	17(1)
S(2)	4c	0.01261(19)	1/4	0.08494(14)	23(1)
S(3)	4c	0.19225(19)	1/4	0.59274(12)	13(1)

Table 3. Atomic coordinates and equivalent isotropic displacement parameters U_{eq} (Å$^2 \times 10^3$) for K$_2$BaTa$_2$S$_{11}$*.

Atom	W.-site	x	y	z	U_{eq}	Occ.
Ta(1)	4e	0.61740(2)	0.38642(3)	0.14028(2)	7(1)	
Ta(2)	4e	0.59501(2)	0.43093(3)	0.33373(2)	8(1)	
Ta(3)	4e	0.14578(2)	0.46205(3)	0.14389(2)	9(1)	
Ta(4)	4e	0.10049(2)	0.44924(3)	0.33372(2)	11(1)	
S(1)	4e	0.72694(15)	0.3220(2)	0.06827(12)	14(1)	
S(2)	4e	0.49093(14)	0.26195(18)	0.10725(11)	11(1)	
S(3)	4e	0.49011(14)	0.39474(18)	0.03737(11)	10(1)	
S(4)	4e	0.63091(15)	0.57856(18)	0.12456(12)	12(1)	
S(5)	4e	0.70547(14)	0.51777(18)	0.22249(11)	10(1)	
S(6)	4e	0.65046(14)	0.27943(18)	0.25957(11)	10(1)	
S(7)	4e	0.47471(14)	0.44143(18)	0.22278(11)	10(1)	
S(8)	4e	0.50384(15)	0.07746(18)	0.21129(11)	11(1)	
S(9)	4e	0.74606(15)	0.4199(2)	0.40364(12)	15(1)	
S(10)	4e	0.67504(16)	0.56255(19)	0.41996(12)	15(1)	
S(11)	4e	0.49352(17)	0.8512(2)	0.08418(13)	19(1)	
S(12)	4e	0.25570(16)	0.3905(2)	0.07857(13)	20(1)	
S(13)	4e	0.06965(15)	0.57574(19)	0.04399(12)	13(1)	
S(14)	4e	0.16381(15)	0.65328(19)	0.12020(12)	13(1)	
S(15)	4e	0.01703(15)	0.33810(19)	0.11601(12)	14(1)	
S(16)	4e	0.10048(16)	0.30177(19)	0.21588(12)	14(1)	
S(17)	4e	0.23935(15)	0.5017(2)	0.26730(12)	15(1)	
S(18)	4e	0.01757(15)	0.55882(19)	0.22994(12)	13(1)	
S(19)	4e	−0.06475(16)	0.4635(2)	0.29281(12)	18(1)	
S(20)	4e	0.0597(2)	0.2914(2)	0.40454(14)	28(1)	
S(21)	4e	0.2008(2)	0.3077(2)	0.38835(16)	29(1)	
S(22)	4e	0.88518(17)	0.0716(2)	0.07353(13)	19(1)	
Ba(1)	4e	0.38369(5)	0.61589(6)	0.10334(4)	12(1)	0.673
K(11)	4e	0.38369(5)	0.61589(6)	0.10334(4)	12(1)	0.327
Ba(2)	4e	0.64731(5)	0.07049(7)	0.07105(4)	14(1)	0.582
K(12)	4e	0.64731(5)	0.07049(7)	0.07105(4)	14(1)	0.418
K(1)	4e	0.85712(8)	0.24723(10)	0.21382(7)	15(1)	0.759
Ba(11)	4e	0.85712(8)	0.24723(10)	0.21382(7)	15(1)	0.241
K(2)	4e	0.85080(9)	0.55027(12)	0.09066(7)	16(1)	0.819
Ba(12)	4e	0.85080(9)	0.55027(12)	0.09066(7)	16(1)	0.181
K(3)	4e	0.10981(11)	0.12155(14)	0.06646(8)	22(1)	0.836
Ba(13)	4e	0.10981(11)	0.12155(14)	0.06646(8)	22(1)	0.164
K(4)	4e	0.33156(15)	0.26216(19)	0.23761(14)	27(1)	0.974
Ba(14)	4e	0.33156(15)	0.26216(19)	0.23761(14)	27(1)	0.026

* Estimated standards deviations are given in parentheses. U_{eq} is defined as one third of the trace of the orthogonalized U_{ij} tensor.

808-666; e-mail: crysdata@fiz-karlsruhe.de, http://www.fiz-informationsdienste.de/en/DB/icsd/depot_anforderung.html) on quoting the deposition numbers CSD-421845 (RbBaTaS$_4$) and CSD-421846 (K$_2$BaTa$_2$S$_{11}$).

Table 4. Selected bond lengths (Å) for RbBaTaS$_4$. Estimated standard deviations are given in parentheses.

Ta – S(1)	2.2494(11) × 2	Ta – S(3)	2.2619(15)
Ta – S(2)	2.2624(18)		

Table 5. Selected bond lengths (Å) for K$_2$BaTa$_2$S$_{11}$. Estimated standard deviations are given in parentheses.

Ta(1) – S(1)	2.262(2)	Ta(1) – S(2)	2.451(2)
Ta(1) – S(4)	2.453(2)	Ta(1) – S(3)	2.4755(19)
Ta(1) – S(5)	2.482(2)	Ta(1) – S(6)	2.502(2)
Ta(1) – S(7)	2.714(2)	Ta(2) – S(11)	2.246(2)
Ta(2) – S(9)	2.427(2)	Ta(2) – S(8)	2.434(2)
Ta(2) – S(10)	2.471(2)	Ta(2) – S(6)	2.484(2)
Ta(2) – S(7)	2.5074(19)	Ta(2) – S(5)	2.845(2)
Ta(3) – S(12)	2.231(2)	Ta(3) – S(13)	2.455(2)
Ta(3) – S(15)	2.457(2)	Ta(3) – S(14)	2.469(2)
Ta(3) – S(16)	2.502(2)	Ta(3) – S(17)	2.507(2)
Ta(3) – S(18)	2.775(2)	Ta(4) – S(22)	2.240(2)
Ta(4) – S(20)	2.447(3)	Ta(4) – S(21)	2.451(3)
Ta(4) – S(19)	2.454(2)	Ta(4) – S(17)	2.500(2)
Ta(4) – S(18)	2.512(2)	Ta(4) – S(16)	2.781(2)
S(2) – S(3)	2.076(3)	S(4) – S(5)	2.097(3)
S(7) – S(8)	2.080(3)	S(9) – S(10)	2.108(3)
S(13) – S(14)	2.076(3)	S(15) – S(16)	2.095(3)
S(18) – S(19)	2.076(3)	S(20) – S(21)	2.103(4)

Physical measurements

Infrared spectroscopy

Infrared spectra in the MIR region (4000 – 400 cm^{-1}; resolution: 2 cm^{-1}) were recorded on a Genesis FT-spectrometer (ATI Mattson). The samples were ground with dry KBr into fine powders and pressed into transparent pellets. Infrared spectra in the far-IR region (550 – 80 cm^{-1}) were collected on an ISF-66 instrument (Bruker) with the samples pressed in polyethylene pellets.

Raman spectroscopy

Raman spectra were recorded on an ISF-66 spectrometer (Bruker) equipped with an additional FRA 106 Raman module. A Nd/YAG laser was used as source (λ = 1064 nm). The samples were ground and prepared on Al sample holders. The measuring range was −1000 to 3500 cm^{-1} (resolution: 2 cm^{-1}).

Solid-state ultraviolet (UV)-visible(Vis)-near-IR spectroscopy

Optical diffuse reflectance measurements were performed at r. t. using a UV-Vis-NIR two-channel spectrometer Cary 5 from Varian Techtron Pty., Darmstadt. The spectrometer is equipped with an Ulbricht sphere (diffuse reflectance accessory; Varian Techtron Pty.). The inner wall of the Ulbricht sphere (diameter 110 mm) is covered with a PTFE layer of 4 mm thickness. A PbS detector (NIR) and a photomultiplier

(UV/Vis) are attached to the Ulbricht sphere. The samples were ground with BaSO$_4$ (as standard for 100 % reflectance) and prepared as a flat specimen. The resolution was 1 nm for the UV/Vis range and 2 nm for the near-IR range. The measuring range was 250 – 2000 nm. Absorption (α/S) data were calculated from the reflectance spectra using the Kubelka-Munk function [38]: $\alpha/S = (1 - R)^2/2R$, where R is the reflectance at a given wave-number, α is the absorption coefficient, and S is the scattering coefficient. The band gap was determined as the intersection point between the energy axis at the absorption offset and the line extrapolated from the linear part of the absorption edge in a $(\alpha/S)^2$ *vs.* E (eV) plot.

Results and Discussion

Synthesis and crystal structures

RbBaTaS$_4$ (**1**)

Compound **1** crystallizes in the orthorhombic space group *Pnma* with one crystallographically independent Rb, Ba, and Ta atom each, as well as three unique S atoms, of which one is located on general position. A view of the structure of compound **1** is presented in Fig. 1. The structure is built up by stacking discrete [TaS$_4$]$^{3-}$ tetrahedra surrounded by Rb$^+$ and Ba^{2+} cations. The [TaS$_4$]$^{3-}$ tetrahedron is slightly distorted, and the Ta–S distances are 2.2494(11) (2 ×), 2.2619(15), and 2.2624(18) Å (average 2.256 Å). The S–Ta–S angles range from 108.20(6) to 110.47(6)°. The bond lengths and angles are in good agreement with those reported for Rb$_3$TaS$_4$ (2.267(3) – 2.282(3) Å) [5]. The Ta–S bonds are short, and one can assume a significant double bond character. Similar short Ta–S bonds from Ta to terminal S atoms are observed in the com-
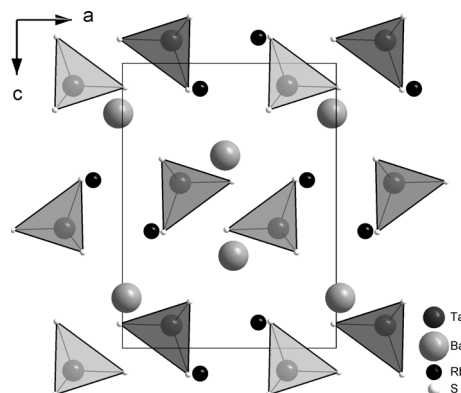

Fig. 1. The arrangement of the [TaS$_4$] tetrahedra and the charge-compensating cations in the crystal structure of RbBaTaS$_4$ with view down [010].
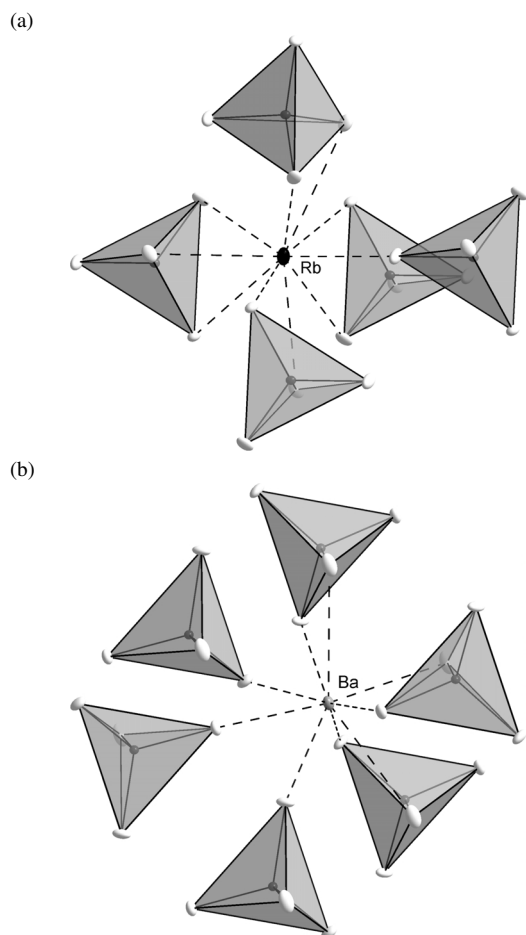
(a)

(b)

Fig. 2. The coordination environments of (a) the Rb cation and (b) the Ba cation. The displacement ellipsoids are drawn at the 50 % probability level.

plex anions [Ta$_2$S$_{11}$]$^{4-}$ (2.228(3) and 2.232(3) Å), [Ta$_4$S$_{22}$]$^{6-}$ (2.208(2) and 2.216(2) Å), [Ta$_4$S$_{25}$]$^{6-}$ (2.208(2) and 2.225(2) Å), and in the compounds Rb$_4$Ta$_2$S$_{11}$ [20], Rb$_6$Ta$_4$S$_{22}$ [27], and Rb$_6$Ta$_4$S$_{25}$ [22], respectively. In these compounds there are also longer Ta–S contacts of 2.442(3) – 2.497(3) Å for Rb$_4$Ta$_2$S$_{11}$ [20], 2.435(2) – 2.543(2) Å for Rb$_6$Ta$_4$S$_{22}$ [27], and 2.429(1) – 2.566(1) Å for Rb$_6$Ta$_4$S$_{25}$ [22]. The longer Ta–S distances are in the single bond range.

With a cut-off at 4.0 Å for Rb–S and Ba–S distances the crystallographically independent Rb$^+$ cations are coordinated by ten S atoms within an irregular polyhedron (Fig. 2). Rb connects five symmetry-related [TaS$_4$]$^{3-}$ anions *via* one (1 ×), two (3 ×), and three (1 ×) S atoms. The Rb–S distances range from 3.277(2) to 3.9394(14) Å with an average of

3.655 Å, longer than the sum of the ionic radii (r_{Rb^+} (CN = 10): 1.66 Å; $r_{S^{2-}}$ = 1.84 Å) [39]. In contrast, Ba^{2+} is surrounded by six symmetry-related [TaS$_4$]$^{3-}$ anions with bonds either to one (3 ×) or three (3 ×) S atoms (Fig. 2). The Ba–S distances (3.2222(18) – 3.7100(17) Å; average: 3.350 Å) are slightly longer than the sum of ionic radii ($r_{Ba^{2+}}$ (CN = 9): 1.47 Å) [39].

It is noted that RbBaTaS$_4$ (**1**) is not isostructural to the analogous K-Nb compound KBaNbS$_4$ [31]. The main difference between the two structures is that KBaNbS$_4$ crystallizes in the (3+1)-dimensional superspace group *Pnma*(α00)0*s*0 with a modulation vector q = (0, 0.629(1), 0), whereas RbBaTaS$_4$ crystallizes in the "normal" orthorhombic space group *Pnma*. A careful inspection shows that RbBaTaS$_4$ (**1**) has a close relationship to the A_2MQ_4 structure type (A = K, Rb, Cs, NH$_4$; M = Mo, W; Q = S, Se) [40 – 47]. The structure of these compounds turns out to be similar to the high-pressure phase of BaF$_2$ [48]. In addition, the structure of **1** can be viewed as an ordered model of Rb$_2$MoS$_4$ [41] with Rb(1) atoms being substituted by Ba atoms, *i. e.*, the Rb and Ba atoms occupy distinct Wyckoff sites, and no mixed occupation of Rb/Ba is observed. The Mo atoms are replaced by the Ta atoms. According to a topological analysis of Blatov [49], in A_2MQ_4 [40 – 47] the Mo or W atoms as the centers of the [MQ_4] tetrahedra form a *hcp* sub-structure. This can be explained by the high formal charge of Mo or W. Repulsive forces between charged Mo^{6+} or W^{6+} ions tend to distribute them as uniformly as possible, which results in a decrease in the energy of their composing matrix and leads to the largest contribution to the stabilization of the crystal lattice. In A_3MQ_4 (A = Na, K, Rb, Cs, Tl, NH$_4$; M = V, Nb, Ta; Q = S, Se) [1 – 11, 50 – 54], the situation is much more complicated. In most of these compounds, for example Rb$_3$TaS$_4$ [5], Ta^{5+} cations form a *fcc* sub-structure, whereas in the structures of Tl$_3$MQ$_4$ (M = V, Ta; Q = S, Se) [50, 51] and Na$_3$MS$_4$ (M = Nb, Ta) [5, 8], the distribution of the V^{5+}, Nb^{5+} or Ta^{5+} cations has a *bcc* sub-structure. In fact, the *bcc* sub-structure of Na$_3$MS$_4$ (M = Nb, Ta) [5, 8] is obviously distorted. This indicates that highly charged cations (Nb^{5+}, Ta^{5+}) tend to separate from each other as far as possible; due to the difference in size between A and M cations, the mixed (M, A) matrices do not follow close-packed patterns. In general, the major contribution to the lattice energy is made by non-directional interatomic interactions [55]. The

dominance of exchange (directional) forces leads to a structural distortion. This can explain the poor uniformity of M^{5+} matrices in the compounds Cu$_3$$MQ_4$ (M = V, Nb, Ta; Q = S, Se) [56 – 60], in which the Q^{2-} anions form *fcc* close packing. Conversely, the *hcp* sub-structure is formed by Ta^{5+} cations in compound **1** due to the large size and higher charge of Ba^{2+} and Rb$^+$ cations.

K$_2$BaTa$_2$S$_{11}$ (2)

Initially the syntheses were performed with the aim to prepare KBaTaS$_4$ *via* the reactive flux method to compare the structure of this hypothetical compound with that of KBaNbS$_4$. Compound **2** was obtained in a reasonable yield by reaction of a mixture of K$_2$S$_3$/BaS/Ta/S in the molar ratio of 1 : 0.75 : 1 : 4. Upon increasing the fraction of BaS, KBaTaS$_4$ was obtained, but unfortunately, crystals of the product were not good enough for single crystal X-ray investigations. Changing the reaction condition such as reaction temperature and cooling rate *etc.* did not improve the quality of the crystals of KBaTaS$_4$, and therefore the single-crystal structure could not be determined. Upon decreasing the fraction of BaS to 0.5, K$_2$Ta$_2$S$_{10}$ [61] was identified as the main product.

Compound **2** crystallizes in the monoclinic space group $P2_1/c$ and is isostructural to K$_2$BaNb$_2$S$_{11}$ [32]. The structure is composed of two different discrete [Ta$_2$S$_{11}$]$^{4-}$ complex anions (Fig. 3) which are well separated by the K$^+$ and Ba^{2+} cations. The anions are arranged in a rod-like manner with alternating
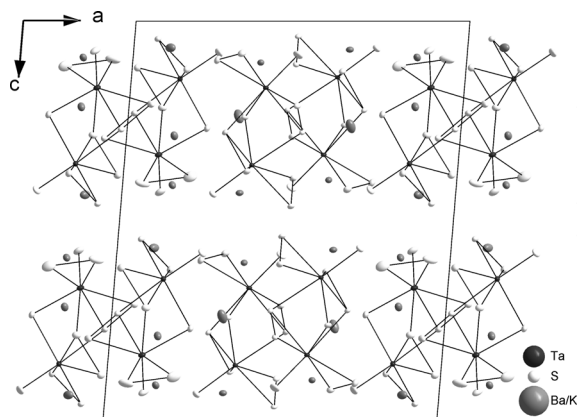
Fig. 3. Arrangement of the [Ta$_2$S$_{11}$]$^{4-}$ anions and the K$^+$/Ba^{2+} cations in the crystal structure of K$_2$BaTa$_2$S$_{11}$ viewed down [010]. The displacement ellipsoids are drawn at the 50 % probability level.

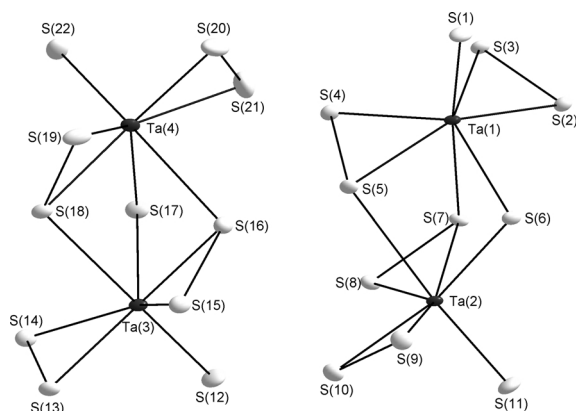Fig. 4. [Ta$_2$S$_{11}$] units in the structure of K$_2$BaTa$_2$S$_{11}$ with atomic labeling. The displacement ellipsoids are drawn at the 50 % probability level.

[Ta(1,2)S$_{11}$]$^{4-}$ and [Ta(3,4)S$_{11}$]$^{4-}$ units along [100]. Each of the two unique anions occurs in "pairs", and along [001] these "pairs" form individual rows. Within the two different [Ta$_2$S$_{11}$]$^{4-}$ anions the shortest Ta–Ta distances (Ta(1)–Ta(2): 3.4763(5) Å; Ta(3)–Ta(4): 3.4461(5) Å) are significantly longer than those in metallic Ta (2.90 Å), indicative of only weak or negligible Ta–Ta interactions. Every Ta atom is coordinated by one terminal monosulfide S^{2-}, one η^2-(S$_2^{2-}$) dianion, one μ^2-S^{2-} unit bridging the two Ta centers, and one additional S$_2^{2-}$ which is η^2-coordinated to one Ta while one S^{2-} of this unit also serves as a second bridging atom to the second Ta center (Fig. 4). Therefore the anion may be described as [Ta$_2$(μ-S)(μ-η^2,η^1-S$_2$)$_2$(η^2-S$_2$)$_2$(S)$_2$]$^{4-}$. In both [Ta$_2$S$_{11}$] groups each Ta atom has a short bond to a terminal S atom (S(1), S(11), S(12), and S(22)) of about 2.2 Å, which may be viewed as a Ta–S double bond. In addition, five medium long Ta–S bonds are between about 2.4 and 2.5 Å (Table 5), and finally, each Ta atom has a longer bond to an S atom of an η^2-S$_2^{2-}$ anion linking neighboring Ta atoms (Ta(1)–S(7): 2.714(2) Å; Ta(2)–S(5): 2.845(2) Å; Ta(3)–S(18): 2.775(2) Å; Ta(4)–S(16): 2.781(2) Å). The average ⟨Ta–S⟩ distances amount to 2.477, 2.488, 2.485, and 2.484 Å for Ta(1), Ta(2), Ta(3) and Ta(4), respectively. These values match well with the sum of the ionic radii (Ta^{5+}: 0.69 Å; S^{2-}: 1.84 Å) [39] and also with the data reported for other compounds with the [Ta$_2$S$_{11}$]$^{4-}$ anion [15, 18 – 20, 25, 27, 61]. The S–S bonds in the S$_2^{2-}$ anions range from 2.076(3) to 2.108(3) Å, typical for S–S single bonds. The [TaS$_7$] polyhedra may be described as

strongly distorted pentagonal bipyramids. The mean deviations of the Ta atoms from the least squares planes defined by S(2)-S(3)-S(4)-S(5)-S(6), S(6)-S(7)-S(8)-S(9)-S(10), S(13)-S(14)-S(15)-S(16)-S(17), and S(17)-S(18)-S(19)-S(20)-S(21) amount to 0.4566(3) Å (Ta(1)), 0.4472(3) Å (Ta(2)), 0.4545(3) Å (Ta(3)), and 0.4298(3) Å (Ta(4)). The angles between the related two "pentagonal planes" are 48.86(4)° and 49.51(4)°, close to those observed in related compounds [15, 18 – 20, 25, 27, 61].

Similar to K$_2$BaNb$_2$S$_{11}$ [32], with a cut-off at about 4.0 Å for K(Ba)–S distances, the coordination numbers for the majority cations are 9 (K(1), Ba(2)), 10 (K(3)), and 11 (K(2), K(4), Ba(1)). In K$_2$BaTa$_2$S$_{11}$ the cations occupy six unique sites with different ratios of Ba^{2+}/K$^+$. The polyhedra around Ba(1)/K(11), Ba(2)/K(12), K(1)/Ba(11), K(2)/Ba(12), K(3)/Ba(13), and K(4)/Ba(14) may also be viewed as a distorted octahedron with 5 S atoms capping triangular faces, a distorted octahedron with two triangle faces capped by S atoms and one edge-sharing S atom, a tricapped trigonal prism, a distorted octahedron with 4 triangular faces capped by S atoms, and a pentacapped trigonal prism, respectively.

A careful comparison with the complex structures of K$_4$Ta$_2$S$_{11}$ [18, 19] and K$_6$Ta$_4$S$_{22}$ [15] shows that compound **2** is closely related to the orthorhombic modification o-K$_4$Ta$_2$S$_{11}$ [19]. The configurations of the [Ta$_2$S$_{11}$]$^{4-}$ anions in both compounds are very similar, but in K$_2$BaTa$_2$S$_{11}$ six unique sites are present for the K$^+$/Ba^{2+} ions (see Table 3) whereas in o-K$_4$Ta$_2$S$_{11}$ only four sites are available. Therefore, the alteration of charges by substituting K$^+$ by Ba$^+$ leads to altered atomic positions, and K$_2$BaTa$_2$S$_{11}$ adopts a different space group. In o-K$_4$Ta$_2$S$_{11}$ the shortest S–S distance between two Ta$_2$S$_{11}$ building blocks is 3.734 Å. In K$_2$BaTa$_2$S$_{11}$ the S(2)–S(8) and S(3)–S(3) separations between neighboring [Ta(1,2)S$_{11}$]$^{4-}$ polyhedra are significantly shorter with 2.955(3) and 2.989(3) Å, and one relatively short contact occurs between adjacent [Ta(3,4)S$_{11}$]$^{4-}$ anions (S(13)–S(13): 3.101(3) Å). Interestingly, the shortest S–S distances between [Ta(1,2)S$_{11}$]$^{4-}$ and [Ta(3,4)S$_{11}$]$^{4-}$ polyhedra are much larger (S(6)–S(14): 3.649(3) Å). This means that there are relatively strong van der Waals interactions between neighboring [Ta(1,2)S$_{11}$]$^{4-}$ and [Ta(3,4)S$_{11}$]$^{4-}$ anions, while such interactions between [Ta(1,2)S$_{11}$]$^{4-}$ and [Ta(3,4)S$_{11}$]$^{4-}$ anions are much weaker. Taking the site occupation factors of the Ba^{2+}/K$^+$ cations, we

find that the environments of the two unique [Ta$_2$S$_{11}$] anions are obviously different. Considering only the Ba^{2+} ions, [Ta(1,2)S$_{11}$]$^{4-}$ is surrounded by 3 Ba(1), 3 Ba(2), 1 Ba(11), 1 Ba(12), 1 Ba(13), and 2 Ba(14) cations. Conversely, only 1 Ba(1) and 1 Ba(2) are found around [Ta(3,4)S$_{11}$]$^{4-}$ together with 2 Ba(11), 3 Ba(12), 3 Ba(13), and 1 Ba(14). This may explain the above mentioned differences of the inter-anionic separations with the smaller Ba^{2+} cation allowing a closer neighborhood between the [Ta(1,2)S$_{11}$]$^{4-}$ anions. Further remarkable differences are found for both the surrounding of the anion by cations and for the polyhedra around the cations between compound **2** and K$_4$Ta$_2$S$_{11}$ [18, 19]. In both o-K$_4$Ta$_2$S$_{11}$ [19] and t-K$_4$Ta$_2$S$_{11}$ [19] the [Ta$_2$S$_{11}$]$^{4-}$ anion is surrounded by 17 K$^+$ ions, and the four unique K$^+$ ions are in heavily distorted tri- or tetracapped trigonal prismatic environments. We note also that compound **2** is much more dense (3.83 g cm^{-3}) than K$_4$Ta$_2$S$_{11}$ (triclinic: 3.18; orthorhombic: 3.28 g cm^{-3}) as a consequence of the significantly different packing of cations and anions.

Optical properties

The solid-state diffuse reflectance UV/Vis spectrum for compound **2** shows a very steep and strong absorption edge at 2.13 eV (Fig. 5), consistent with the transparent red-orange color. The absorption edge is caused by a transition from the top of the valence band (VB) to the bottom of the conduction band (CB), where the upmost part of the valence band can be presumably attributed to S (3p) states, and the bottom of the conduction band results most likely from empty Ta (5d)
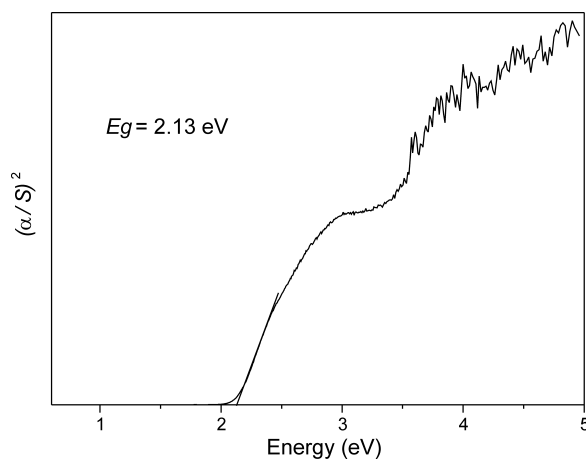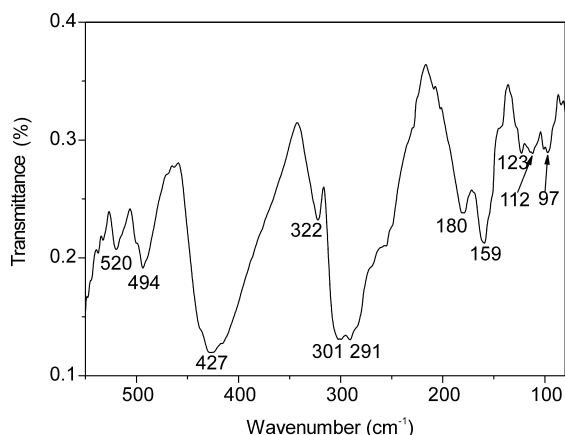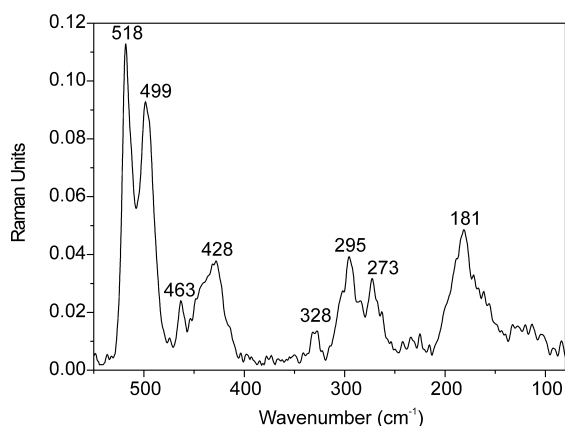

Fig. 5. Transformed reflectance spectrum of K$_2$BaTa$_2$S$_{11}$.

Fig. 6. Far-IR spectrum of K$_2$BaTa$_2$S$_{11}$.

Fig. 7. FT-Raman spectrum of K$_2$BaTa$_2$S$_{11}$.

orbitals. Compared to those of K$_4$Ta$_2$S$_{11}$ [18, 19], the value for the band gap has decreased by 0.2 ~ 0.3 eV in compound **2** due to the introduction of Ba^{2+} in the structure.

The far-IR and Raman spectra for K$_2$BaTa$_2$S$_{11}$ (**2**) in the range of 80 to 550 cm^{-1} are shown in Figs. 6 and 7. Due to the resonance Raman effect, the spectra exhibit a significant dependence on the excitation frequency. With the Nd-YAG laser excitation line (λ = 1064 nm), which is far away from the first electronic absorption band at 582 nm corresponding to the band gap of 2.13 eV, a "normal" or at best pre-resonance Raman spectrum is observed. The S–S stretching vibrations (ν(S–S)) at 518 and 499 cm^{-1} of the very polarizable disulfide ligands is the most intense band in the Raman spectrum (Fig. 7). The assignment of ν(S–S) is supported by the bands at 520 and 494 cm^{-1} in the complementary far-IR spectrum (Fig. 6). According to

the selection rules, no distinct absorption is detected around 500 cm^{-1}. The large hypsochromic shift of ν(S–S) of the coordinated disulfide ligands correlates well with the distinctly shorter S–S distances (2.076(3) to 2.108(3) Å) as compared with those (S–S: 2.112(8) to 2.138(5) Å) in K$_2$S$_2$ (ν(S–S) = 475 and 453 cm^{-1}) [62] and are similar to those (2.064(2) to 2.105(2) Å) in K$_2$BaNb$_2$S$_{11}$ (ν(S–S) = 522 and 499 cm^{-1}) [32]. The peaks at 463 and 428 cm^{-1} in the Raman spectrum and the broad band at 427 cm^{-1} in the far-IR spectrum are assigned to the symmetric ν_s(Ta–S$_t$) and anti-symmetric ν_{as}(Ta–S$_t$) stretching vibrations of the terminal sulfide ions, respectively. Compared to the spectra of K$_2$BaNb$_2$S$_{11}$ [32], the peaks at 328 and 295 cm^{-1} with a shoulder at higher energy in the Raman spectrum are due to the symmetric ν_s(Ta–S$_\mu$) stretching mode of the Ta–S–Ta bridge that is split into two bands by the interaction with other Ta–S stretching modes. Correspondingly, the modes at 301 and 291 cm^{-1} in the IR spectrum are assigned to the antisymmetric vibration of such Ta–S–Ta bridges. The absorptions at 322 cm^{-1} (IR) and 273 cm^{-1} (Raman) are mixed Ta–S vibrations which are also related to the Ta–S–Ta bridge. Compared to K$_2$BaNb$_2$S$_{11}$ [32], the signals at 180 cm^{-1} (IR) and 181 cm^{-1} (Raman) can be assigned to the lowest energy ν(Ta–S) vibrations. All peaks below 160 cm^{-1} in both the Raman and the IR spectrum are due to S–Ta–S bending vibrations.

Conclusions

Our efforts to synthesize and characterize new thiotantalates within the quaternary system *A*/Ba/Ta/S have led to the new compounds RbBaTaS$_4$ and K$_2$BaTa$_2$S$_{11}$, which crystallize isotypically to Rb$_2$MoS$_4$ [41] and K$_2$BaNb$_2$S$_{11}$ [32]. The different occupations of Rb$^+$ and Ba^{2+} in the structure of RbBaTaS$_4$ lead to the formation of a *hcp* sub-structure. This sub-structure was also observed for KBaNbS$_4$ [32], but both structures are different. The reason why the structure of KBaNbS$_4$ exhibits a small modulation which is not observed for RbBaTaS$_4$ cannot yet be explained. Similar to K$_2$BaNb$_2$S$_{11}$, the occurrence of the statistically occupied Ba^{2+}/K$^+$ cation sites in K$_2$BaTa$_2$S$_{11}$ leads also to two distinct [Ta$_2$S$_{11}$]$^{4-}$ anions, which are surrounded by different numbers of Ba^{2+} or K$^+$ cations. Compared to the pure potassium compounds, the decrease of the optical band gap demonstrates the influence of the Ba^{2+} ions.

[1] K. O. Klepp, G. Gabl, *Eur. J. Solid State Inorg. Chem.* **1997**, *34*, 1143.

[2] J. M. van den Berg, R. de Vries, *Proc. K. Ned. Akad. Wet. Ser. B Phys. Sci.* **1964**, *67*, 178.

[3] P. Dürichen, W. Bensch, *Eur. J. Solid State Inorg. Chem.* **1996**, *33*, 309.

[4] M. Emirdag-Eanes, J. A. Ibers, *Z. Kristallogr. NCS* **2001**, *216*, 489.

[5] R. Niewa, G. V. Vajenine, F. J. DiSalvo, *J. Solid State Chem.* **1998**, *139*, 404.

[6] M. Latroche, J. A. Ibers, *Inorg. Chem.* **1990**, *29*, 1503.

[7] O. Krause, C. Näther, I. Jess, W. Bensch, *Acta Crytallogr.* **1998**, *C54*, 902.

[8] S. Herzog, C. Näther, P. Dürichen, W. Bensch, *Z. Anorg. Allg. Chem.* **1998**, *624*, 2021.

[9] S. Herzog, C. Näther, W. Bensch, *Acta Crystallogr.* **1998**, *C54*, 1742.

[10] B. Deng, J. A. Ibers, *Acta Crystallogr.* **2004**, *E60*, i147.

[11] H. Yun, C. R. Randall, J. A. Ibers, *J. Solid State Chem.* **1988**, *76*, 109.

[12] W. Bensch, P. Dürichen, *Eur. J. Solid State Inorg. Chem.* **1996**, *33*, 527.

[13] W. Bensch, P. Dürichen, *Eur. J. Solid State Inorg. Chem.* **1996**, *33*, 1233.

[14] W. Bensch, P. Dürichen, *Inorg. Chim. Acta* **1997**, *261*, 103.

[15] P. Stoll, C. Näther, W. Bensch, *Z. Anorg. Allg. Chem.* **2002**, *628*, 2489.

[16] W. Bensch, P. Dürichen, *Z. Anorg. Allg. Chem.* **1996**, *622*, 1963.

[17] K. O. Klepp, G. Gabl, *Z. Naturforsch.* **1998**, *53b*, 1236.

[18] S. Schreiner, L. E. Aleandri, D. Kang, J. A. Ibers, *Inorg. Chem.* **1989**, *28*, 392.

[19] S. Herzog, C. Näther, W. Bensch, *Z. Anorg. Allg. Chem.* **1999**, *625*, 969.

[20] P. Dürichen, W. Bensch, *Acta Crystallogr.* **1998**, *C54*, 706.

[21] P. Stoll, C. Näther, I. Jeß, W. Bensch, *Acta Crystallogr.* **2000**, *C56*, 368.

[22] P. Stoll, C. Näther, I. Jeß, W. Bensch, *Solid State Sci.* **2000**, *2*, 563.

[23] P. Dürichen, M. Bolte, W. Bensch, *J. Solid State Chem.* **1998**, *140*, 97.

[24] O. Tougait, J. A. Ibers, *Solid State Sci.* **1999**, *1*, 523.

[25] C. L. Teske, W. Bensch, *Z. Anorg. Allg. Chem.* **2001**, *627*, 385.

[26] C. L. Teske, W. Bensch, *Acta Crystallogr.* **2006**, *E62*, i26.

[27] P. Stoll, C. Näther, I. Jeß, W. Bensch, *Z. Anorg. Allg. Chem.* **2000**, *626*, 959.

[28] W. Bensch, P. Dürichen, C. Näther, *Solid State Sci.* **1999**, *1*, 85.

[29] O. Krause, P. Dürichen, C. Näther, W. Bensch, *Solid State Sci.* **2000**, *2*, 197.

[30] P. Dürichen, W. Bensch, *Z. Naturforsch.* **2002**, *57b*, 1382.

[31] Y. D. Wu, T. Doert, W. Bensch, *Z. Anorg. Allg. Chem.* **2005**, *631*, 3019.

[32] Y. D. Wu, C. Näther, N. Lehnert, W. Bensch, *Solid State Sci.* **2005**, *7*, 1062.

[33] Y. D. Wu, C. Näther, W. Bensch, *J. Solid State Chem.* **2007**, *180*, 113.

[34] G. M. Sheldrick, *Acta Crystallogr.* **1990**, *A46*, 467; *ibid.* **2008**, *A64*, 112.

[35] L. M. Gelato, E. Parthè, *J. Appl. Crystallogr.* **1987**, *20*, 139.

[36] A. L. Spek, *J. Appl. Crystallogr.* **2003**, *36*, 7.

[37] Y. Le Page, *J. Appl. Crystallogr.* **1988**, *21*, 983.

[38] P. Kulbelka, F. Munk, *Z. Tech. Phys.* **1931**, *12*, 593.

[39] R. D. Shannon, *Acta Crystallogr.* **1976**, *A32*, 751.

[40] M. Emirdag-Eanes, J. A. Ibers, *Z. Kristallogr. NCS* **2001**, *216*, 484.

[41] J. Ellermeier, C. Näther, W. Bensch, *Acta Crystallogr.* **1999**, *C55*, 1748.

[42] C. C. Raymond, P. K. Dorhout, S. M. Miller, *Z. Kristallogr.* **1995**, *210*, 775.

[43] J. Lapasset, N. Chezeau, P. Belougne, *Acta Crystallogr.* **1976**, *B32*, 3087.

[44] H. Schäfer, A. Weiss, G. Schäfer, *Z. Naturforsch.* **1964**, *19b*, 76.

[45] J. Y. Yao, J. A. Ibers, *Acta Crystallogr.* **2004**, *E60*, i10.

[46] B. R. Srinivasan, C. Näther, W. Bensch, *Acta Crystallogr.* **2007**, *E63*, i167.

[47] B. R. Srinivasan, M. Poisot, C. Näther, W. Bensch, *Acta Crystallogr.* **2004**, *E60*, i136.

[48] J. M. Leger, J. Haines, A. Atouf, O. Schulte, S. Hull, *Phys. Rev. B* **1995**, *52*, 13247.

[49] M. V. Peskov, V. A. Blatov, *Russ. J. Inorg. Chem.* **2006**, *51*, 590.

[50] C. Crevecoeur, *Acta Crystallogr.* **1964**, *17*, 757.

[51] M. Vlasse, L. Fournes, *C. R. Hebd. Seances Acad. Sci. C* **1978**, *287*, 47.

[52] H. Schäfer, P. Moritz, A. Weiss, *Z. Naturforsch.* **1965**, *20b*, 603.

[53] Y. K. Do, E. D. Simhon, R. H. Holm, *Inorg. Chem.* **1985**, *24*, 4635.

[54] O. Krause, C. Näther, W. Bensch, *Acta Crystallogr.* **1999**, *C55*, 1197.

[55] E. V. Peresypkina, V. A. Blatov, *Acta Crystallogr.* **2003**, *B59*, 361.

[56] C. Mujica, G. Carvajal, J. Llanos, O. Wittke, *Z. Kristallogr. NCS* **1998**, *213*, 12.

[57] M. Kars, A. Rebbah, H. Rebbah, *Acta Crystallogr.* **2005**, *E61*, i180.

[58] A. E. van Arkel, C. Crevecoeur, *J. Less-Common Metals* **1963**, *5*, 177.

[59] K. O. Klepp, D. Gurtner, *Z. Kristallogr. NCS* **2000**, *215*, 4.

[60] Y. J. Lu, J. A. Ibers, *J. Solid State Chem.* **1993**, *107*, 58.

[61] Y. D. Wu, C. Näther, W. Bensch, *J. Solid State Chem.* **2005**, *178*, 1569.

[62] P. Böttcher, J. Getzschmann, R. Keller, *Z. Anorg. Allg. Chem.* **1993**, *619*, 476.